

International Journal of Medical Engineering and Informatics

ISSN online: 1755-0661 - ISSN print: 1755-0653
<https://www.inderscience.com/ijmei>

Spotting congenital heart diseases using palm print based on faster R-CNN and spatial method

Y. Mahesha, C. Nagaraju

DOI: [10.1504/IJMEI.2022.10044267](https://doi.org/10.1504/IJMEI.2022.10044267)

Article History:

Received: 22 June 2021
Accepted: 07 November 2021
Published online: 22 December 2023

Spotting congenital heart diseases using palm print based on faster R-CNN and spatial method

Y. Mahesha* and C. Nagaraju

The National Institute of Engineering,
Visvesvaraya Technological University,
Mysore, Karnataka, India

Email: maheshyg029@gmail.com

Email: nagaraj@nie.ac.in

*Corresponding author

Abstract: This paper proposes a machine learning method to detect congenital heart diseases (CHDs) using a palm pattern known as axial triradius. This article spreads light on three things. First, Faster R-CNN Inception v2 has been used to identify triradii on the palm image. Secondly, a novel spatial method has been proposed to select leftmost, rightmost and axial triradii. Finally, the angle at axial triradius has been calculated on the palm images of healthy people and of patients suffering from tetralogy of Fallot (TOF), atrial septal defect (ASD), ventricular septal defect (VSD) and coarctation of aorta (CoA). The result shows that the proposed method can be used as a screening method to predict CHDs.

Keywords: axial triradius; CHDs; faster R-CNN; inception v2; spatial method.

Reference to this paper should be made as follows: Mahesha, Y. and Nagaraju, C. (2024) 'Spotting congenital heart diseases using palm print based on faster R-CNN and spatial method', *Int. J. Medical Engineering and Informatics*, Vol. 16, No. 1, pp.56–70.

Biographical notes: Y. Mahesha obtained his Bachelor's in Information Science and Engineering in 2010 and then he obtained his Master's in Computer Science and Engineering in 2012 from PES College of Engineering, Karnataka, India. He is pursuing his PhD in Visvesvaraya Technological University, Karnataka, India. Currently, he is working as an Assistant Professor in the Department of Computer Science and Engineering, Mysuru Royal Institute of Technology, Karnataka, India. His specialisations are in the field of image processing and machine learning.

C. Nagaraju received his BE degree from Mysore University, Karnataka and M Tech degree from Visvesvaraya Technological University, Karnataka. He was awarded PhD from Mysore University, Karnataka. Currently, he is working as an Assistant Professor in the Department of Electronics and Communication, The National Institute of Engineering, Karnataka. His research interest includes medical image processing and artificial intelligence. He has published 13 research publications in refereed international journals. He is a reviewer of some of the international journals.

1 Introduction

In the modern era, people are suffering from different kinds of diseases. Among these, some are life-threatening. The disease which is related to the heart is a matter of high concern because heart disease often leads to sudden death. The cause of heart disease is either genetically related or a baleful lifestyle. Heart disease which is genetically related is known as congenital heart disease (CHD). A few common CHDs are Fallot's tetralogy (FT) (Khan et al., 2019), atrial septal defect (ASD) (Celermajer, 2018), ventricular septal defect (VSD) (Cox et al., 2020) and coarctation of aorta (COA) (Rogers and Clawson, 2019). Since the CHD is genetically related, the research works were carried out to find the correlation between different types of CHDs and patterns on palm print.

Sanchez cascos initiated the work on the detection of CHDs using a palm pattern known as axial triradius (Cascos, 1965). He analysed palm prints of 150 patients and palm prints of 50 normals. He concluded that patients suffering from FT have their axial triradius located at a more distal position than normal. Takashina and Yorifuji (1966) presented a study to find the correlation between CHD and axial triradius. After the experiment, they come up with the conclusion that axial triradius is found at the distal position more in CHD patients than in acquired heart disease patients. Alter and Schulenberg (1970) conducted a study on dermatoglyphics in CHDs. From the results obtained, the author has confirmed the conclusions of previous research works that the patients suffering from FT tend to have a large angle at axial triradius compared to healthy people. David (1981) continued the work of previous researchers with palm prints of males and females. The study has justified the work of previous researchers that axial triradius is in a more distal position in diseased than in the normal. Brijendra et al. (2016) experimented on the palm prints of 150 patients and palm prints of 300 normals. They arrived with the same conclusion as previous researchers and concluded that axial triradius is in a more distal position in diseased than in normal. Mahesha and Nagaraju (2020) conducted a survey on work carried out by doctors to find the relationship between palm patterns and CHDs. The conclusions made by the previous researchers on the detection of CHDs using axial triradius are given in Table 1.

Table 1 'atd' angle for CHDs

<i>Researcher</i>	<i>CHD</i>	<i>'atd' angle</i>
Sanchez Cascos	Fallot's tetralogy (FT)	> 46°
N Pushpamala	Atrial septal defect (ASD)	> 46°
Singh Brijendra	Ventricular septal defect (VSD)	> 51°
	TOF and COA	> 45°

The major limitations of previous research works are, they are dealt with ink palm print and patterns on the palm print were identified through eyes. The parameters required to detect CHDs were evaluated manually using geometrical instruments such as scale and protractor. Working with digital palm print is more efficient than using ink palm print. The angle at axial triradius can be obtained using a template matching algorithm (Mahesha and Nagaraju, 2021). The limitation in template matching based method to detect triradii is manual cropping of templates in each palm image to locate the triradii. So far, a machine learning-based method has been adopted to detect the palm patterns such as ulnar loop and whorl. Hence, this article is proposing a machine learning method

to automate the identification of the location of triradii and finding the position of axial triradius which is used as a parameter to detect CHDs.

2 Material and methods

2.1 *Faster R-CNN-based approach to detect triradii*

The architecture adopted to detect the triradii on palm images is based on Faster R-CNN (Ren et al., 2017; Xiao et al., 2020). The architecture consists of two parts. One is region proposal network (RPN) and another one is bounding box classifier. The RPN generates region proposals from the feature map. The bounding box classifier detects the triradii in an input palm image after getting the region proposals as input from RPN.

2.1.1 *Region proposal network*

RPN takes a palm image as an input and generates rectangular regions each with an objective score. To generate region proposals, a small network slides over the convolutional feature map. This small network takes the $n \times n$ spatial window of a convolutional feature map and maps to a lower-dimensional feature. This feature is fed into two fully connected layers namely the box regression layer and box classification layer.

At each sliding window location, k number of region proposals generated. Hence, the regression layer has $4k$ outputs and the classification layer has $2k$ outputs. The region proposals are parameterised relative to reference boxes, which are called anchors. An anchor is centred and is associated with a scale and aspect ratio.

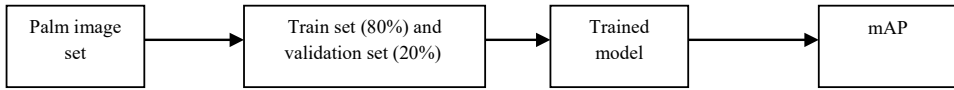
A binary class label is used for each anchor for training RPNs. The positive label has been assigned to two kinds of anchors:

- 1 the anchors with the highest intersection-over-union (IoU) overlap with a ground truth box
- 2 an anchor that has an IoU overlap higher than 0.7 with any ground-truth box.

2.1.2 *Training and validation*

The steps involved in the training and validation process are shown in Figure 1.

- *Palm image set*: The palm print images have been collected in such a way that the patterns should be visible on the palm image. 100 palm images have been selected for training and validating the system.
- *Train and validation set*: The palm image dataset is divided into train and validation sets. 80% of the images have been used for training. 20% of the images have been used to validate the system.
- *Trained model*: The model has been trained to detect the triradii on the palm image by setting hyper-parameter values.

Figure 1 Training and validation

2.1.3 Detection of triradii on palm image using Faster R-CNN

Bounding boxes around the triradii are generated through the following two steps

- 1 In the first step, the anchor boxes are generated at each location by the RPN. Fully connected layers find the location of anchor boxes. Also, computes the probability that the anchor box belongs to the class and the background.
- 2 In the second step, a collection of region of interest (ROI) is generated. These regions pass through a pooling layer and fully connected layers. The bounding boxes are refined. The location of triradii in the output images is determined by the bounding boxes.

The centre of the rectangular box detected on the palm image is the actual triradius. Coordinate values of the top left corner and bottom right corner are used to find the location of the centre of the rectangle.

2.1.4 Selection of leftmost, rightmost and axial triradii using the spatial method

Normally, the palm image has five triradii. All these triradii are detected by the proposed model. The proposed model detects the bounding boxes around all the triradii. The centres of the bounding boxes are the locations of triradii. For the detection of CHD, the angle at axial triradius is required. The angle at axial triradius is calculated using equation (1).

$$\theta = \cos^{-1} (ta \cdot td) / (|ta| \cdot |td|) \quad (1)$$

where 'ta' is the vector towards the leftmost triradius from axial triradius, 'td' is the vector towards the rightmost triradius from axial triradius and 'θ' is the angle at the axial triradius. This equation needs the position of the leftmost triradius, rightmost triradius and the axial triradius. To get the bounding boxes around the leftmost, rightmost and axial triradii, the following procedure is used.

The spatial arrangement of bounding boxes on the image appears as shown in Figure 2.

- 1 The left-most bounding box has the least value for the minimum and maximum x-coordinate value.
- 2 The rightmost bounding box has the highest value for the minimum and maximum x-coordinate value.
- 3 The bottom bounding box has the highest value for the minimum and maximum y-coordinate value.

The centres of the leftmost bounding, rightmost bounding box and bottom bounding box are the leftmost, rightmost and axial triradii respectively as shown in Figure 3.

Figure 2 Spatial arrangement of bounding boxes (see online version for colours)

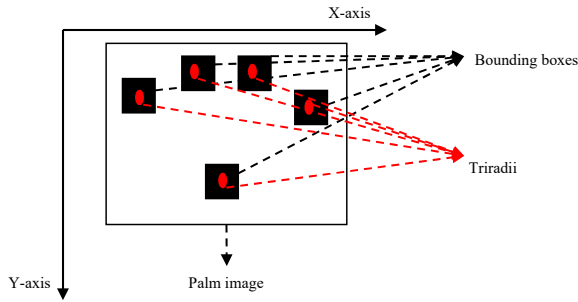
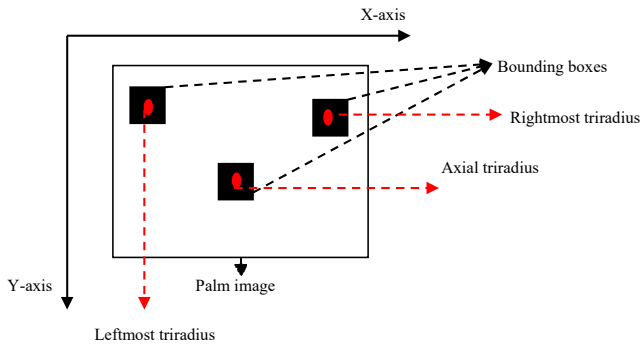


Figure 3 Detection of leftmost, rightmost and axial triradii (see online version for colours)



3 Results

The results obtained from the proposed system are explained below. Palm images have been collected in such a way that patterns on the palm should be visible. A sample of the palm images taken in the study is shown in Figure 4. The resolution of images taken is 1,074 * 1,333.

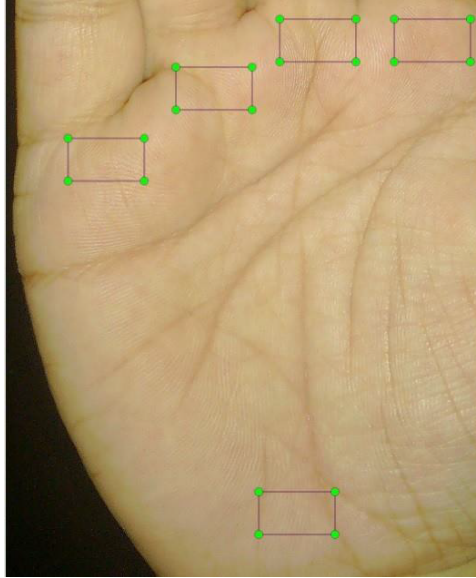
Figure 4 Sample palm image (see online version for colours)



3.1 Labelling

The triradii are labelled on the train palm images as shown in Figure 5. The annotated objects are of rectangle shape. The centre of the rectangle is the actual triradius.

Figure 5 Labelling of triradii (see online version for colours)



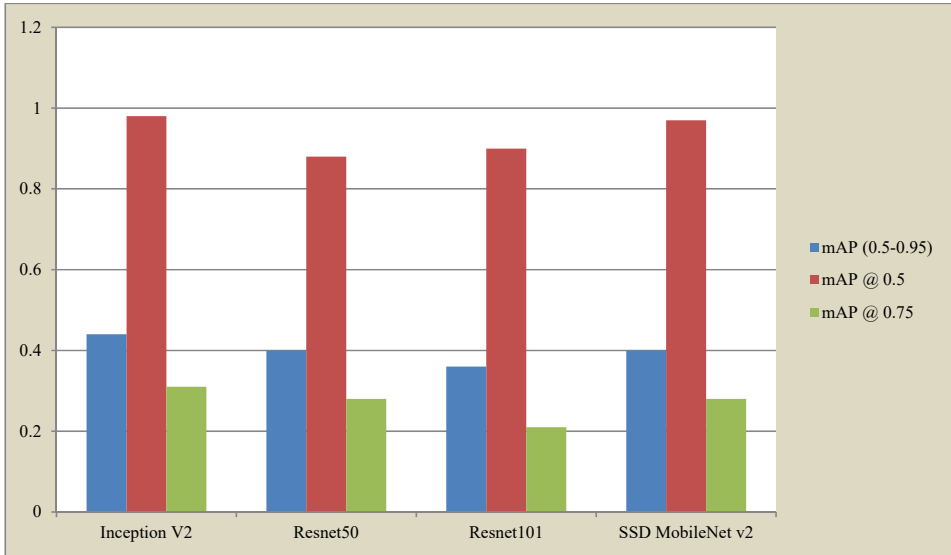
3.2 Training

The system has been trained using different methods to generate feature maps. The final result obtained for each of the feature extraction methods is given in Table 2 and Figure 6. An IoU score > 0.5 is normally used for analysing the models and hence mAP at IoU > 0.5 has been taken for comparison among different object detection models. Figure 7 shows the mean average precision (mAP) (Henderson and Ferrar, 2016; Oksuz et al., 2018) obtained for the validation set across different steps during the training process for different feature map generation methods.

Table 2 Mean average precision

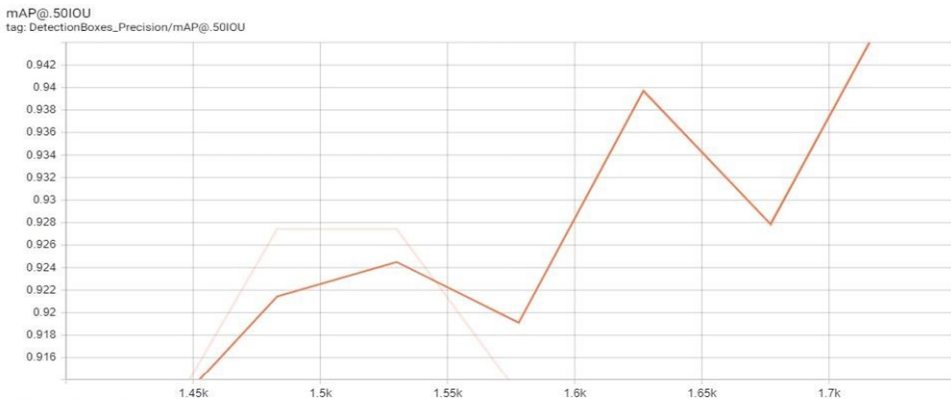
<i>Model</i>	<i>Method used to generate feature map</i>	<i>mAP (0.5–0.95)</i>	<i>mAP @ 0.5</i>	<i>mAP @ 0.75</i>
Faster	Inception v2	0.44	0.98	0.31
R-CNN	Resnet 50	0.40	0.88	0.28
	Resnet 101	0.36	0.90	0.21
SSD	Mobilenet v2	0.40	0.97	0.28

Figure 6 Mean average precision resulted from different object detection models (see online version for colours)



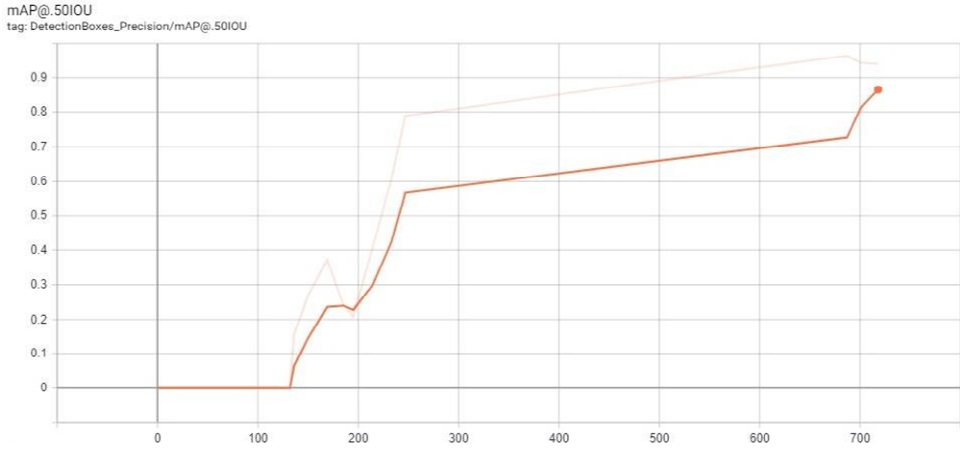
From the results obtained as shown in Table 2 and Figure 7, it is found that Faster R-CNN is giving better mAP at IoU > 0.5 with inception v2 compared to resnet 101 (Oksuz et al., 2018; Butt et al., 2020) and resnet 50 (He et al., 2016; Nath and Kushagra, 2020). Also, Faster R-CNN gives slightly better performance than SSD Mobilenet v2 (Howard et al., 2017; Sandler et al., 2018) in the detection of triradii. Hence, in the detection of triradii, inception v2 has been adopted with Faster R-CNN.

Figure 7 mAP for different detection models, (a) mAP obtained from inception v2 (b) mAP obtained from resnet50 (c) mAP obtained from resnet101 (d) mAP obtained SSD Mobilenet v2 (see online version for colours)

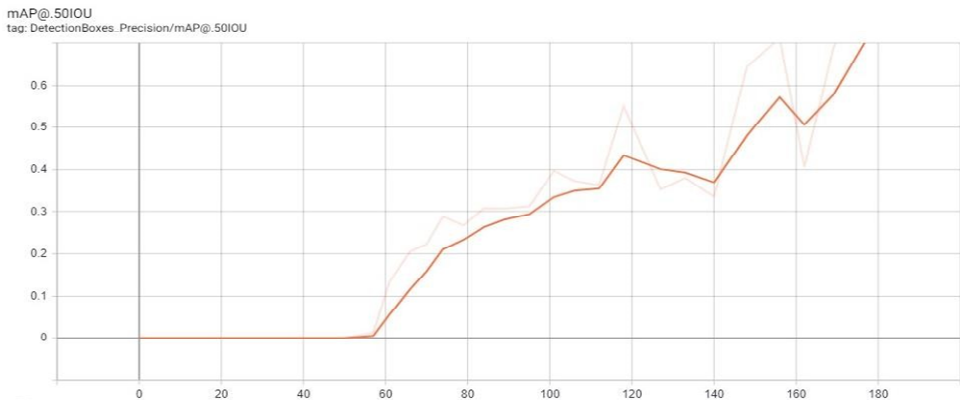


(a)

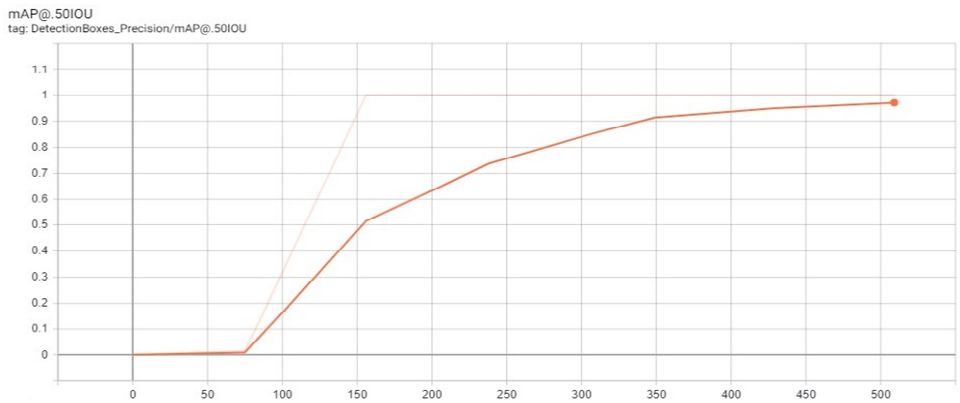
Figure 7 mAP for different detection models, (a) mAP obtained from inception v2 (b) mAP obtained from resnet50 (c) mAP obtained from resnet101 (d) mAP obtained SSD Mobilenet v2 (continued) (see online version for colours)



(b)



(c)



(d)

3.3 Detection of triradii

The bounding boxes around the triradii on palm images are detected as shown in Figure 8. The system takes the palm image as input. The inception block generates the feature map. The feature map passes through the RPN. The RPN generates region proposals and these region proposals are provided as input to the box classifier. The box classifier forms bounding boxes around all the triradii on the output palm image.

Figure 8 Detection of triradii (see online version for colours)

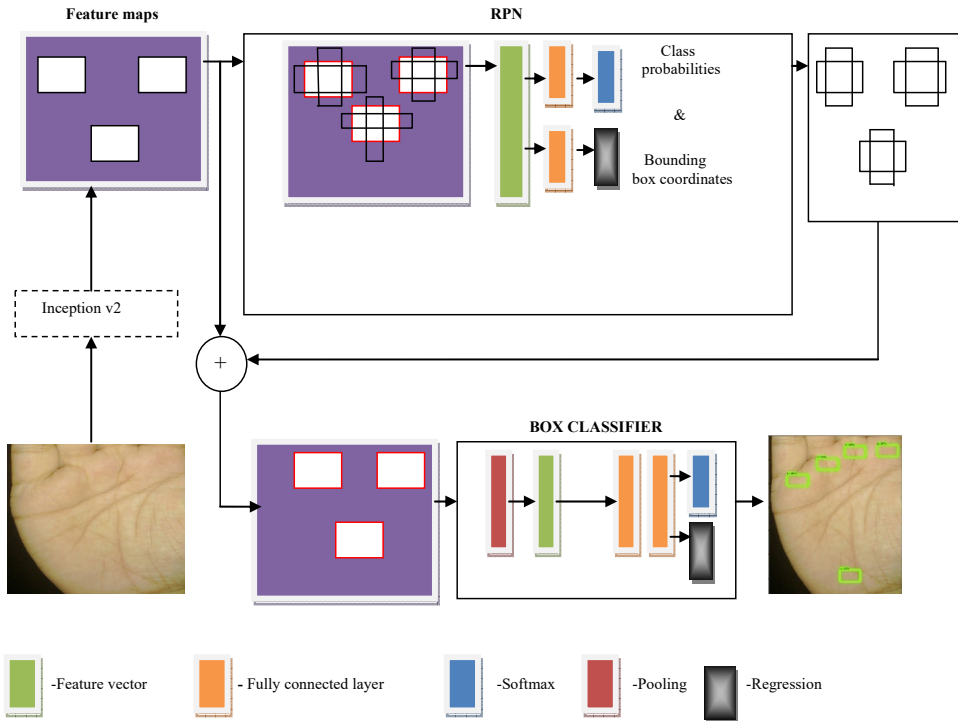
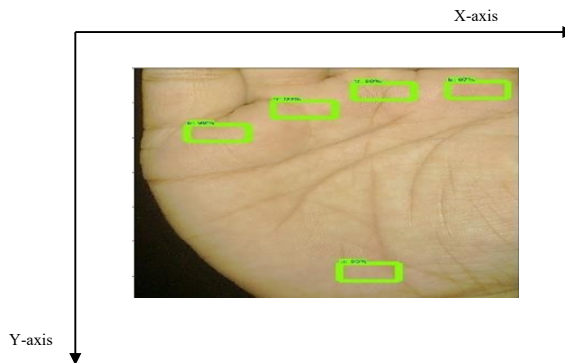


Figure 9 The spatial arrangement of bounding boxes (see online version for colours)



The centre of each of the bounding boxes shown in Figure 9 detected on the palm image represents the triradius. The positions of leftmost, rightmost and axial triradii are needed to find the angle at axial triradius. These positions are obtained by finding the centres of leftmost, rightmost and bottom bounding boxes.

The leftmost, rightmost and bottom bounding boxes are selected using the spatial method as shown in Figure 10. Positions of these corners of the bounding boxes are given in Table 3.

Figure 10 Leftmost, rightmost and bottom bounding boxes (see online version for colours)

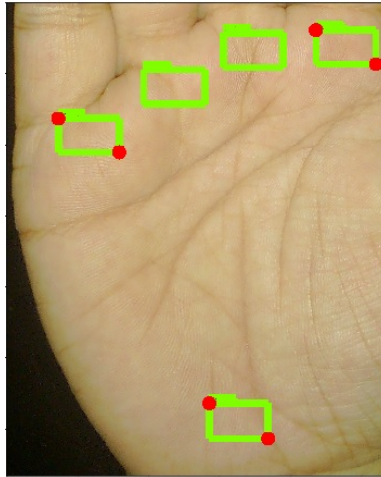
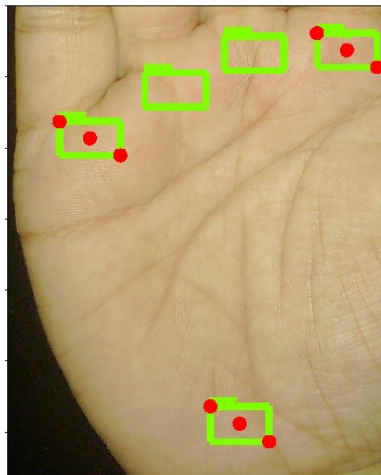


Figure 11 Position of leftmost, rightmost and axial triradius (see online version for colours)



The centres of the leftmost, rightmost and bottom bounding boxes were evaluated using equation (2).

$$\begin{aligned} centre_x &= \frac{x_{\min} + x_{\max}}{2} \\ centre_y &= \frac{y_{\min} + y_{\max}}{2} \end{aligned} \quad (2)$$

These centres represent the positions of leftmost, rightmost and axial triradii as shown in Figure 11 and the coordinate values of positions are presented in Table 4.

Table 3 Position of corners of bounding boxes

	<i>Xmin</i>	<i>Ymin</i>	<i>Xmax</i>	<i>Ymax</i>
Leftmost bounding box	147	327	319	422
Rightmost bounding box	874	78	1043	174
Bottom bounding box	573	1129	739	1228

Table 4 Position of triradii

<i>Triradius</i>	<i>Position</i>
Leftmost triradius	(233,374)
Rightmost triradius	(958,126)
Axial triradius	(656,1178)

3.4 Detection of CHDs

Palm images have been collected from 156 TOF patients, 86 ASD patients, 112 VSD patients, 74 CoA patients and 100 healthy people. The proposed method has been applied to find the angle at axial triradius and the results obtained are shown in Table 5.

Table 5 Verification of 'atd' angle

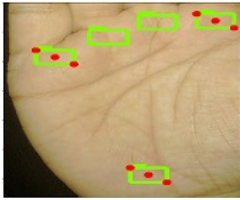
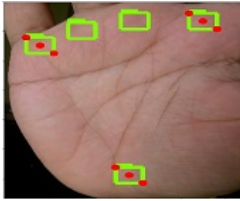
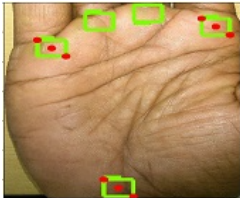
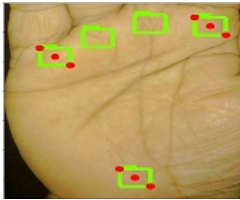
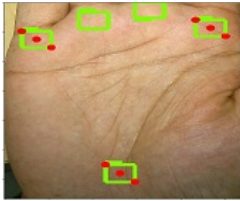
<i>Type of CHD</i>	<i>Number of people considered for the study</i>	<i>Number of people with 'atd' angle in the following range</i>			
		<i><45°</i>	<i>>45° and <46°</i>	<i>>46° and <51°</i>	<i>>51°</i>
ASD	86	06	21	46	13
VSD	112	12	19	8	73
CoA	74	03	35	18	06
TOF	156	08	102	12	34
Healthy	100	74	12	00	14

From the results given in Table 5, it is found that ASD patients tend to have 'atd' angle in the range $> 46^\circ$ and $< 51^\circ$, VSD patients tend to have 'atd' angle $> 51^\circ$, CoA patients tend to have 'atd' angle in the range $> 45^\circ$ and $< 46^\circ$, TOF patients tend to have 'atd' angle in the range $> 46^\circ$ and $< 51^\circ$ and healthy people tends to have 'atd' angle $< 45^\circ$. Table 6 shows false negative (FN), false positive (FP), true positive (TP), true negative (TN) and accuracy for each of the specified CHDs. The application of the proposed method on sample palm images taken from the dataset is shown in Table 7.

Table 6 Accuracy of prediction

	<i>Range of 'atd' angle used for prediction</i>	<i>FN</i>	<i>FP</i>	<i>TP</i>	<i>TN</i>	<i>Accuracy</i>
86 ASD patients, 100 healthy	> 46° and < 51°	40	00	46	100	78.5%
112 VSD patients, 100 healthy	> 51°	39	14	73	86	75%
74 COA patients, 100 healthy	> 45° and < 46°	27	12	35	88	70.70%
156 TOF patients, 100 healthy	> 45° and < 46°	54	12	102	88	74.21%

Table 7 Prediction of CHDs on sample images (see online version for colours)

<i>Input image</i>	<i>Output image</i>	<i>'atd' angle</i>	<i>Actual</i>	<i>Prediction</i>
		45.39	Suffering from TOF	Possibly suffering from CoA and TOF
		35.12	Normal	Normal
		52.18	Suffering from VSD	Possibly suffering from VSD
		42.21	Normal	Normal
		47.18	ASD	Possibly suffering from ASD

4 Discussion

The present article proposes a machine learning method to detect CHDs using angle at axial triradius. Faster R-CNN-based method has been adopted to detect triradii on palm images. The experiment has been carried out with three different feature extraction methods such as Inception v2, Resnet50 and Resnet101. A set of 100 palm images were used to conduct the experiment. These 100 images were divided into train and validation sets. The proposed system has been provided training using the bounding boxes around the triradii of train images. The centre of each boundary box is the actual triradii. The mAP has been evaluated for the validation set. The mAP at IoU > 0.5 has been considered to compare the performance of different feature extraction methods used with Faster R-CNN and also to compare Faster R-CNN with SSD Mobilenet v2. The mAP values for Inception v2, Resnet50 and Resnet101 are 0.98, 0.88 and 0.90, respectively. From the results obtained, it is found that faster R-CNN performs better with Inception v2 in the detection of triradii. In the second part of the research work, a novel spatial method has been proposed to select the leftmost, rightmost and axial triradius. These triradii are essential to finding the angle at the axial triradius. Finally, palm images were collected from patients suffering from TOF, ASD, VSD and CoA. Palm images were collected from healthy people also. The angle at axial triradius was calculated for the diseased and healthy using the proposed method. The result obtained is presented in Table 5 and Table 6. The result shows that angle at axial triradius can be used to detect CHDs.

5 Conclusions

A machine learning method has been proposed to detect CHDs using angle at axial triradius. The proposed method uses Faster R-CNN to detect triradii on palm images. From the experimental results, it is found that Faster R-CNN shows better performance with Inception v2 compared to Resnet50 and Resnet101. Also, Faster R-CNN shows slightly better performance compared to SSD MobileNet v2. The mAP obtained for Faster R-CNN Inception v2 is 0.98 at IoU > 0.5. To find the angle at axial triradius, leftmost, rightmost and axial triradii are required. Hence, a novel spatial method has been proposed to select these three triradii. The angle at axial triradius was calculated on palm images of CHD patients and Healthy people using Faster R-CNN Inception v2. The result shows that the proposed method can be used as a screening method to detect CHDs such as TOF, VSD, ASD and CoA. Since the proposed model is cost-effective it can be used to test the possibility of CHDs in economically backward countries. The CHDs also have a strong association with other palm patterns such as whorl, loop and arches. Hence, in future, the proposed method may be used to experiment on detection of palm patterns other than triradii and this may contribute to detect some other CHDs.

References

- Alter, M. and Schulenberg, R. (1970) 'Dermatoglyphics in congenital heart disease', *Circulation*, Vol. 41, No. 1, pp.49–54, <https://doi.org/10.1161/01.CIR.41.1.49>.
- Brijendra, S., Renu, G., Dushyanth, A., Rajneesh, G. and Sunil, K. (2016) 'Dermatoglyphic's in congenital cardiac disease', *Acta Medica Iranica*, Vol. 54, No. 2, pp.119–123.
- Butt, A.M., Yousaf, M.H., Murtaza, F., Nazir, S., Viriri, S. and Velastin, S.A. (2020) 'Agglomerative clustering and residual-VLAD encoding for human action recognition', *Applied Sciences*, Vol. 10, No. 12, p.4412, DOI: 10.3390/app10124412.
- Cascos, A.S. (1965) 'Palmprint pattern in congenital heart disease', *British Heart Journal*, Vol. 27, No. 4, pp.599–603, DOI: 10.1111/j.1651-2227.1968.tb07277.x.
- Celermajer, D.S. (2018) 'Atrial septal defects: even simple congenital heart diseases can be complicated', *European Heart Journal*, Vol. 39, No. 12, pp.999–1001, DOI: 10.1093/eurheartj/ehx633.
- Cox, K., Algaze-Yojay, C., Punn, R. and Silverman, N. (2020) 'The natural and unnatural history of ventricular septal defects presenting in infancy: an echocardiography-based review', *Journal of the American Society of Echocardiography*, Vol. 33, No. 6, pp.763–770, DOI: 10.1016/j.echo.2020.01.013.
- David, T.J. (1981) 'Dermatoglyphics in congenital heart disease', *Journal of Medical Genetics*, Vol. 18, No. 5, pp.344–349, DOI: 10.1136/jmg.18.5.344.
- He, K., Zhang, X., Ren, S. and Sun, J. (2016) 'Deep residual learning for image recognition', in *2016 IEEE Conference on Computer Vision and Pattern Recognition*, IEEE, December, pp.770–778, DOI: 10.1109/CVPR.2016.90.
- Henderson, P. and Ferrari, V. (2016) 'End-to-end training of object class detectors for mean average precision', in *13th Asian Conference on Computer Vision*, Springer, November, pp.198–213, DOI: 10.1007/978-3-319-54193-8_13.
- Howard, A.G., Zhu, M., Chen, B. and Kalenichenko, D. (2017) *MobileNets: Efficient Convolutional Neural Networks for Mobile Vision Applications*, arXiv:1704.04861v1[cs.CV].
- Khan, S.M., Drury, N.E., Stickley, J., Barron, D.J., Brawn, W.J., Jones, T.J., Anderson, R.H. and Crucean, A. (2019) 'Tetralogy of Fallot: morphological variations and implications for surgical repair', *Eur. J. Cardiothorac. Surg.*, Vol. 56, No. 1, pp.101–109, DOI: 10.1093/ejcts/ezy474.
- Mahesha Y. and Nagaraju, C. (2021) 'Automating the identification and evaluation of the position of axial triradius on palm print: an approach to early detection of congenital heart diseases', *Biomedical Engineering: Applications, Basis and Communications*, Vol. 33, No. 2, p.2150021, DOI: 10.4015/S1016237221500216.
- Mahesha, Y. and Nagaraju, C. (2020) 'A literature review on analysis of palm print patterns to detect congenital heart disease', *Biomedical Engineering: Applications, Basis and Communications*, Vol. 32, No. 2, p.2050012, DOI: 10.4015/S101623722050012X.
- Nath, U. and Kushagra, S. (2020) *Better Together: Resnet-50 Accuracy with 13x Fewer Parameters and at 3x Speed*, arXiv:2006.05624v1[cs.LG].
- Oksuz, K., Cam, B.C., Akbas, E. and Kalkan, S. (2018) 'Localization recall precision (LRP): a new performance metric for object detection', in *15th European Conference on Computer Vision*, Springer, September, pp.521–537, DOI: 10.1007/978-3-030-01234-2_31.
- Ren, S., He, K., Girshick, R. and Sun, J. (2017) 'Faster R-CNN: towards real-time object detection with region proposal networks', *IEEE Transactions on Pattern Analysis and Machine Intelligence*, Vol. 39, No. 6, pp.1137–1149, DOI: 10.1109/TPAMI.2016.2577031.
- Rogers, C. and Clawson, R.E. (2019) 'Coarctation of the aorta', *Journal of the American Academy of Physician Assistants*, Vol. 32, No. 6, pp.46–47, DOI: 10.1097/01.JAA.0000558245.81325.02.

- Sandler, M., Howard, A., Zhu, M., Zhmoginov, A. and Chen, L-C (2018) 'MobileNetV2: inverted residuals and linear bottlenecks', *2018 IEEE/CVF Conference on Computer Vision and Pattern Recognition*, IEEE, December, pp.4510–4520, DOI: 10.1109/CVPR.2018.00474.
- Takashina, T. and Yorifuji, S. (1966) 'Palmar dermatoglyphics in heart disease', *The Journal of the American Medical Association*, Vol. 197, No. 9, pp.689–692, DOI: 10.1001/jama.1966.03110090053016.
- Xiao, Y., Wang, X., Zhang, P., Meng, F. and Shao, F. (2020) 'Object detection based on faster R-CNN algorithm with skip pooling and fusion of contextual information', *Sensors (Basel)*, Vol. 20, No. 19, p.5490, DOI: 10.3390/s20195490.